

Semiconducting BaS₃ phase featuring v-shape S₃ unit at high pressureSheng Wang,¹ Siyu Liu,¹ Pengyue Gao,^{1,*} Jian Lv,¹ Yanchao Wang^{1,†} and Guochun Yang^{2,‡}¹State Key Laboratory of Superhard Materials and International Center of Computational Method & Software, College of Physics, Jilin University, Changchun 130012, China²State Key Laboratory of Metastable Materials Science & Technology and Key Laboratory for Microstructural Material Physics of Hebei Province, School of Science, Yanshan University, Qinhuangdao 066004, China

(Received 20 December 2021; revised 22 February 2022; accepted 23 March 2022; published 19 April 2022)

Pressure-induced structural transformation of known compounds has become an effective routine to obtain new materials. The sulfur motifs that are present in compounds have a considerable effect on their crystal structures and electronic properties. Here, we focus on exploring the evolution of S motifs in the BaS₃ compound under high pressure. A novel P3₁21-BaS₃, consisting of an equivalent V-shape S₃ unit and quasi-hexagon Ba ring, is identified through the combination of first-principles swarm-intelligence search and phonon softening calculations. The bond angle in the S₃ unit decreases, accompanied by pressure-induced structural phase transition. P3₁21-BaS₃ shows a semiconducting character, mainly originating from the contribution of S 3*p*-electron states. Along with the newly proposed BaS₃ structure, the temperature effect on stability is estimated using the temperature-dependent effective potential method. For another S-rich BaS₂, the disappearance of the S₂ unit induced by pressure (> 150 GPa) is mainly responsible for structural instability.

DOI: [10.1103/PhysRevResearch.4.023046](https://doi.org/10.1103/PhysRevResearch.4.023046)

I. INTRODUCTION

Pressure, as a fundamental thermodynamic parameter, plays an irreplaceable role in triggering chemical reaction, stabilizing functional materials, and inducing structural phases that are inaccessible at ambient conditions [1–4]. As a typical representative, pressure-induced hydrides such as H₃S [5–7] and LaH₁₀ [8,9] exhibit remarkable high superconducting transition temperatures, approaching the dream of room-temperature superconductivity. On the other hand, pressure can also induce extraordinary changes in chemical attributes and oxidation states of atoms, which are of great importance for fundamental science and application research. For instance, Cs in pressure-induced CsF₅ demonstrates the attribute of *p*-blocking elements [10], and Au in Li₄Au acts as a 6*p*-element [11]. Pressure-induced OsF₈ and IrF₈ break the limits of transition-metal fluorination [12,13], achieving a +8 oxidation state of Os and Ir, and they have extremely high electron affinity.

As for *s*-block alkali-earth elements, they have high chemical reactivity, but invariably +2 oxidation state. Ba, as the heaviest nonradioactive-decay member of alkali-earth metals, demonstrates the strongest relativistic effect and reactive activity [14]. At high pressure, Ba also shows unusual chemical characters. The reaction of Ba with F can activate its inert

5*p*-electrons, showing a high oxidation state greater than +2 [15]. Ba₃S₂ is predicted to be stable at above 40.2 GPa, in which Ba exhibits the mixture valence states of Ba⁺ and Ba²⁺ [16]. BaCl exhibits ferromagnetism, rarely observed in main-group elements, which can be attributed to pressure-induced *s*-*d* transition in the Ba atom [17].

The alkali-earth metal chalcogenide compounds *M_xCh_y* (*M* = Mg, Ca, Sr, Ba, and *Ch* = O, S, Se, Te) are technologically important materials exhibiting widespread applications, such as in microelectronics, light-emitting diodes, and magneto-optical devices [18–20]. On the other hand, chalcogenide species (e.g., *Ch*₂²⁻, *Ch*²⁻, *Ch*³⁻) in this kind of compound arouse considerable scientific interest, especially at high pressure. Pressure-induced CaO₃ and CaS₃ contain V-shape trimeric O₃²⁻ and S₃²⁻ units, respectively [21–23]. The formal charge of O₃²⁻ in CaO₃ is in sharp contrast to O₃⁻ in KO₃ at ambient pressure [24]. More interesting, the finding of CaO₃ offers insights for elucidating prominent seismic anomalies and oxygen cycles in Earth's interior. Additionally, S is in favor of the formation of diverse motifs (e.g., dimer, trimer, chain, and ring) in S-rich compounds that show interesting properties and applications [25–29].

Taking into account these considerations, we explore the potential S-rich BaS₃ and BaS₂ compounds with the aim of finding novel S motifs. We conducted structural search for BaS₃ and BaS₂ at high pressures and found a new P3₁21-BaS₃ phase deriving from the predicted P3₂21-BaS₃ induced by phonon softening at 100 GPa. A *Fd-3m*-BaS₂ structure was found at 150 GPa, which is identical with the phase transition result of the P4₁2₁1-BaS₂ structure at the corresponding pressure. The favorable motifs in the two compounds are V-shape S₃ and dumbbell S₂, respectively. We found a distinct structural feature of the Ba layers modulated by the S₃ units in the two BaS₃ phases. Besides determining the crystalline structure, we also systemically investigate

*Corresponding author: gpy@calypso.cn†Corresponding author: wyc@calypso.cn‡Corresponding author: yanggc468@nenu.edu.cn

the temperature effect on the structure and stability of BaS_2 and BaS_3 .

II. METHOD

The crystal structure predictions of BaS_2 and BaS_3 at 50, 100, and 150 GPa were performed by the in-house-developed particle swarm optimization method as implemented in the CALYPSO package, which has been proved to be an efficient tool for discovering unprecedented materials only with given pressures and chemical compositions [30,31]. Part of the predicted compounds have been experimentally confirmed, leading to breakthrough findings such as conventional high-temperature superconductors [4,32–34]. All of the geometrical optimizations and property simulations were carried out using the projector augmented-wave [35] method with Perdew-Burke-Ernzerhof [36] exchange correlation function in the Vienna ab initio simulation package [37]. The $5s^25p^66s^2$ and $3s^23p^4$ serve as the valence electrons for Ba and S, respectively. The kinetic cutoff energy of the plane waves was set to 600 eV, and appropriate Monkhorst-Pack k-meshes were chosen to guarantee the enthalpy of the simulated system converging to 1 meV/atom. To check the dynamical stability of the proposed structures, phonon dispersion curves were carried out using the finite displacement method as implemented in the PHONOPY code [38,39]. The temperature-dependent effective potential (TDEP) method was used to estimate the finite-temperature effect [40–42].

III. RESULTS AND DISCUSSION

The known BaS_3 phase with $P\text{-}42_1m$ symmetry was readily reproduced at 50 GPa [16], validating the reliability of our adopted structural prediction and geometry optimization methods, which make our following work more convincing. In a recent study, Li *et al.* [16] proposed a BaS_3 phase with $C2$ symmetry becoming more energetically favorable than the already known $P\text{-}42_1m$ phase at a pressure greater than approximately 75 GPa. We propose a new BaS_3 phase crystallizing in $P3_121$ symmetry with six formula units ($Z = 6$) at 100 GPa, having a lower enthalpy than that of the ones proposed by Li *et al.* at corresponding pressures [Fig. 1(a)]. Notably, we did not find the structure in a straightforward manner through the structural search calculations. The original structure obtained from the structural search is the one having $P3_221$ symmetry with three formula units ($Z = 3$). However, $P3_221\text{-BaS}_3$ is dynamically unstable in view of the presence of imaginary phonon vibration modes at point A [Fig. 1(b)] along the high symmetry path, indicating that this phase is not a local minimum structure. Subsequently, the frozen-phonon calculations were performed to investigate whether there exists a more stable structure derived from the $P3_221\text{-BaS}_3$ phase induced by the soft mode. The enthalpy is calculated as a function of the corresponding atomic displacements along or opposite to the eigenvector of the soft mode at point A, while the other parameters maintain the values in the parent structure. Notably, the points equivalent to point A resulting from the rotational operations corresponding to the $P3_121$ space group are also discussed in Supplemental

Material (Supplemental Material Fig. S2) [43]. As shown in Fig. 1(c), two equivalent enthalpy minima were explored on the path of the structure going through, indicating that there appear to be two structures derived from the $P3_221\text{-BaS}_3$ phase with six formula units (6 f.u.). Further analysis confirms that the two structures are identical, named as $P3_121\text{-BaS}_3$. On the other hand, we also carried out a structural search with 6 f.u. The previously mentioned $P3_121\text{-BaS}_3$ phase is readily identified in the structural search (see Supplemental Material [43]), which confirms the reliability of our adopted soft-mode method.

It is intriguing to investigate the details of the transition from the structure corresponding to the saddle point [$P3_221\text{-BaS}_3$, Fig. 1(c)] of the potential energy surface (PES) to the one corresponding to the local minimum. As shown in Fig. 2(a), the $P3_221\text{-BaS}_3$ phase consists of 12 S atoms forming a ring, with an S-S distance of ~ 2.11 Å. There are two types of S atoms inside the ring—named S1 [represented by yellow sphere in Fig. 2(a)] and S2 (represented by the orange sphere), respectively. As Fig. 2(a) shows, in the $P3_221\text{-BaS}_3$ structure, one S2 atom links to four S1 atoms, while one S1 atom links to two S2 atoms, demonstrating an alternant arrangement. As mentioned earlier, the unstable $P3_221\text{-BaS}_3$ structure will transfer to the stable one with a lower symmetry $P3_121$, driven by phonon softening at point A. Once the $P3_221$ structure is expanded along the c direction, it is obvious that the Ba atoms keep their positions.

We carefully analyzed the phase transition process as illustrated in Fig. 2(a). The S2 atoms have tiny movements along the eigenvector of the soft mode (indicated by the black arrows) to form the S_3 unit (in $P3_121$). The dashed black lines indicate the broken bonds resulting from the movements. Combined with Fig. 1(c), it is clearly seen that the S2 atom linking to two S1 atoms is energetically preferable rather than linking to four S1 atoms, leading to the breaking of the S ring and accompanied by the appearance of the S_3 units with an S-S-S angle of 98.6° (e.g., V-shape S_3 unit) and an S-S distance of ~ 2.03 Å that is slightly shorter than ~ 2.11 Å in the $P3_221$ phase. The absence of imaginary frequency modes in the whole Brillouin zone of the $P3_121\text{-BaS}_3$ phase [Fig. 1(d)] indicates its dynamical stability. On the other hand, the bond angle of the S_3 unit in the two BaS_3 phases becomes smaller with pressure (e.g., 115.1° for $P\text{-}42_1m$ at 0 GPa, and 98.6° for $P3_121$ at 100 GPa).

$P3_121\text{-BaS}_3$ contains two inequivalent Ba atoms—Ba1 and Ba2—occupying the 3b (0.1428, 0.0000, 0.8333) and 3a (0.1497, 0.0000, 0.3333) sites, and consists of three inequivalent S atoms sitting at the 6c (0.6791, 0.4761, 0.1308), 6c (0.6829, 0.4921, 0.6344), and 6c (0.4096, 0.9586, 0.0881) positions. Both Ba1 and Ba2 are surrounded by 12 S atoms forming polyhedra with 15 faces. We named the edge (or center) S atom in the S_3 unit as S1 (or S2), which follows the same name in the S ring of the $P3_221\text{-BaS}_3$ structure. From the side view [Fig. 2(b)], Ba atoms could be considered as a layer-like structure, but with a quite short interlayer distance of about 2.78 Å, with the S_3 unit staying upon or beneath the layers alternatively. From the top view, Ba atoms form a hexagon ring [Fig. 2(b)] with a tiny distortion relative to the adjacent layers. We employ Bader charge analysis to identify

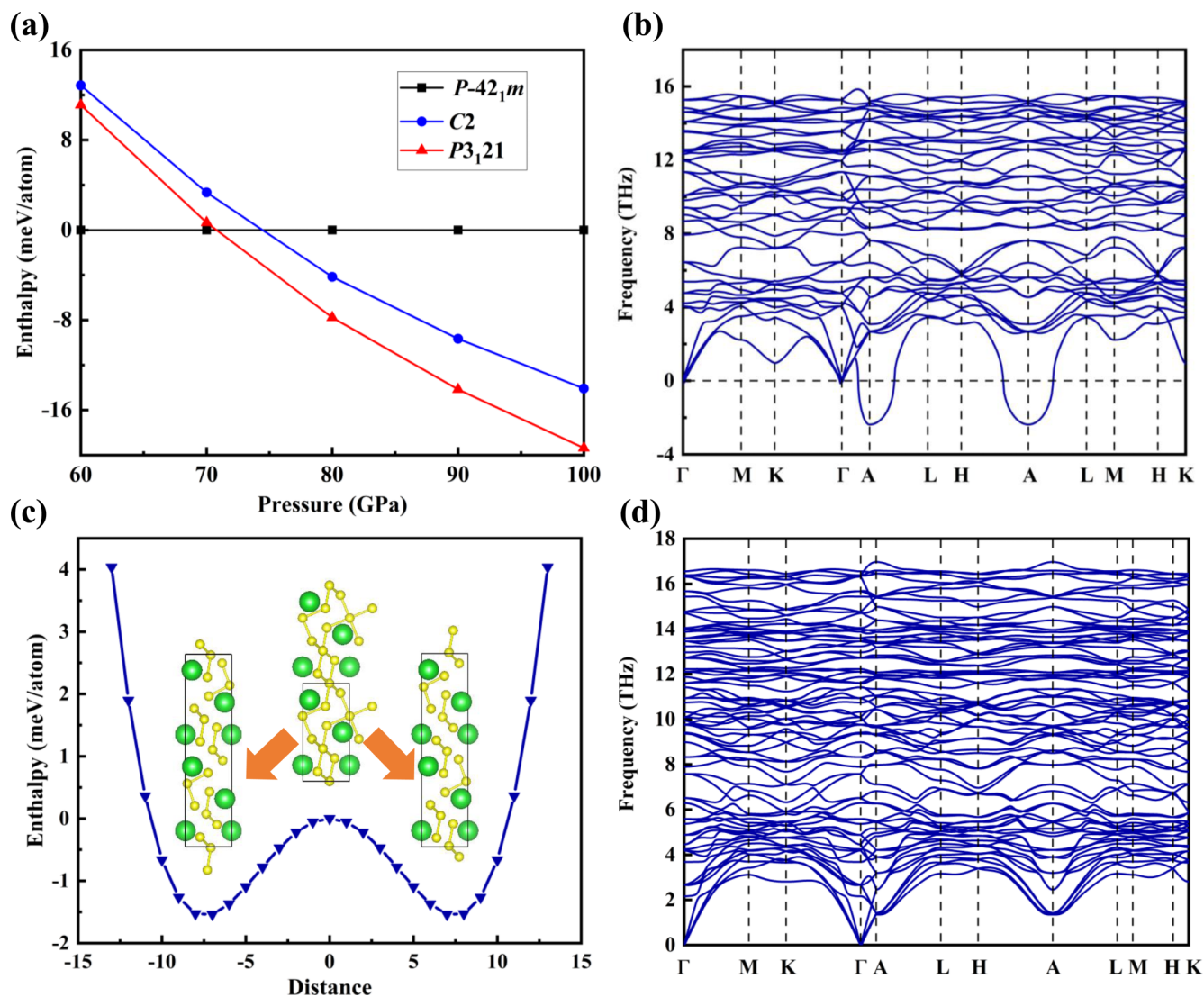


FIG. 1. (a) Enthalpy differences per atom as a function of pressure for the conventional $P-421m$, previously proposed $C2$, and the newly predicted $P3_{121}$ phases, where the enthalpies of the $P-421m$ phase at the considered pressure points are chosen as the basis. (b) The phonon dispersion relations of the predicted $P3_{121}$ phase show a large image frequency at point A. (c) Enthalpy evolution as a function of the atom displacement induced by the soft mode corresponding to point A of the high-symmetry path at a pressure of 100 GPa for the $P3_{121}$ -BaS₃ structure. Inset figures show the two equivalent structures with $P3_{121}$ symmetry corresponding to the two equivalent local minima of the PES. (d) Phonon spectra of $P3_{121}$ -BaS₃ derived from the unstable $P3_{121}$ structure induced by the soft mode.

the number of transferring electrons from the Ba atom to the S atom. Generally, Bader analysis underestimates the electron transfer value, thus we selected the CsCl-type BaS compound as a standard, in which the Ba atom is considered to lose all the s -orbital electrons, inducing S to show a -2 state. As illustrated in Table I, each of the two edge S1 atoms acquires approximately one electron, while the center S2 atom barely gains an electron. Combined with the electron localization functions (ELF) analysis [Fig. 2(c)], it is clearly seen that each edge S1 atom gains one electron from three adjacent Ba atoms. As mentioned earlier, it is clearly seen that one Ba atom is surrounded by six S1 atoms, and, in reverse, one S1 atom is surrounded by three Ba atoms. Therefore, it is reasonable to consider that the both valence electrons of the Ba atom are divided without bias by the six S1 atoms, indicating one S1 atom obtains $1/3$ ($2/6$) electrons from each Ba atom,

which confirms the inner-layer hexagonal configuration of the Ba atoms.

To gain more quantitative insight into the S-S bonding states, we also calculated the crystalline orbital Hamiltonian population (COHP) and integrated crystalline orbital Hamiltonian population (ICOHP) to characterize the S—S bond in the S₃ unit and the S ring. The S—S bond between the S1 and S2 atom in the S₃ unit and the corresponding one in the S ring are chosen in the COHP and ICOHP calculations. The appearance of the large bonding states and small antibonding states [Fig. 3(a)] below the Fermi level reveals that bonding interaction in the S₃ unit and the S ring is strong. However, the bonding interaction in the S₃ unit is slightly stronger than in the S ring, which implies the instability of the $P3_{121}$ structure and prefers to form the S₃ unit in the BaS₃ compound at high pressure. On the other hand, the weak S2-S1 bonding

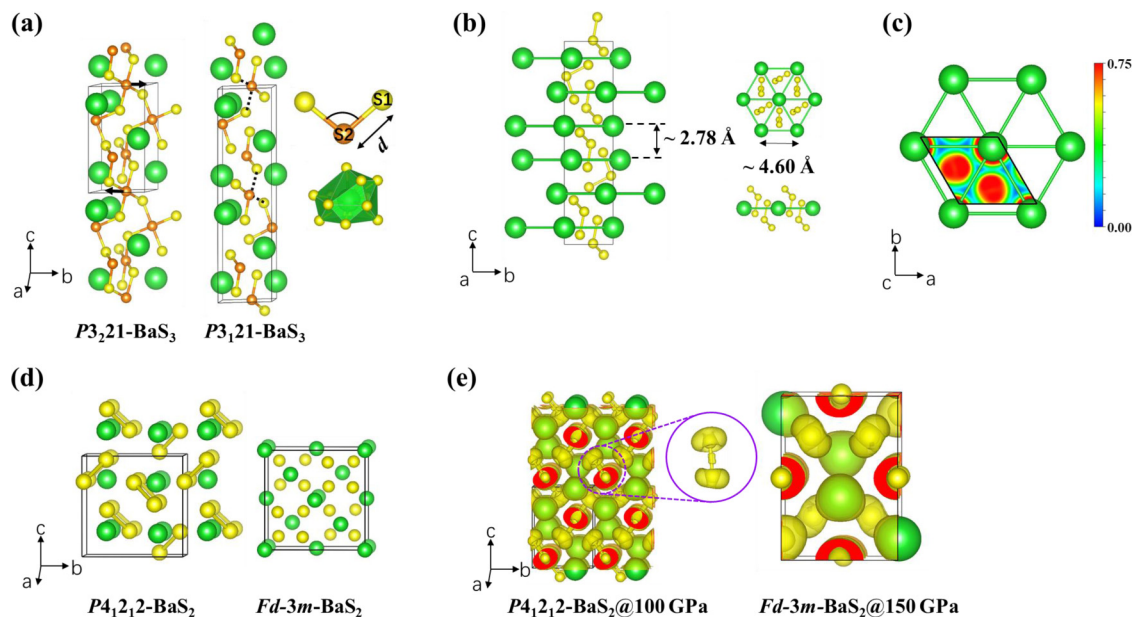


FIG. 2. (a) The crystal structures of the BaS_3 structure with $P3_21$ and $P3_121$ symmetry. Large green and small yellow (orange) spheres represent the Ba and S1 (S2) atoms, respectively. The black arrows indicate two of the S2 atoms moving along the eigenvector of the soft phonon mode, and the black dashed line shows the broken bond induced by atomic movement. (b) Side view (along the a -axis) and the top view of the stable $P3_121$ - BaS_3 phase. (c) Calculated ELF of $P3_121$ - BaS_3 on the (001) plane is used to confirm the hexagonal configuration of the Ba atoms and (d) the $P4_12_12$ - BaS_2 structure proposed by Li *et al.* [16] at 100 GPa (left) and the $Fd-3m$ - BaS_2 structure at 150 GPa (right). To distinguish the S_2 units, we reduced the Ba radius. (e) The ELF results of the $P4_12_12$ - BaS_2 compound at 100 GPa and $Fd-3m$ - BaS_2 at 150 GPa. The image in the large purple circle shows the localized electron in the S—S bond.

interaction and S2 atom located at the center of four S1 atoms in $P3_21$ - BaS_3 could lead to the vibration of S2 at a finite temperature. Subsequently, we investigated the effect of the finite temperature through performing *ab initio* molecular dynamics (AIMD) simulations at 300 K with the TDEP method. The stability of the $P3_21$ - BaS_3 structure at a temperature of 300 K can be illustrated by the calculated phonon dispersion curve [Fig. 3(c)], in which there is no imaginary frequency in the whole high-symmetry path, throwing light on the $P3_21$ - BaS_3 phase with the S ring could be synthesized at high-temperature and high-pressure conditions.

Moreover, in addition to the $P3_121$ - BaS_3 structure, we found another BaS_3 structure (space group $P3_21$, 6 formula units). The enthalpy difference between the two phases is less than 1.5 meV/atom. To distinguish the two phases, the newly found structure is named T - BaS_3 {here, T means the trigonal system; Supplemental Material Fig. S3(b) [43]}, also consisting of the S_3^{2-} unit as it appeared in $P3_121$ - BaS_3 . However, the Ba atoms in T - BaS_3 are arranged in a different stacking order along the c -axis, as shown in Supplemental Material Fig. S3(a) and (b) [43].

TABLE I. Bader charges in CsCl-type BaS , $P3_21$, and $P3_121$ - BaS_3 at a pressure of 100 GPa.

	Ba	S/S1	S2
BaS	1.10	-1.10	
$P3_21$ - BaS_3	1.15	-0.55	-0.05
$P3_121$ - BaS_3	1.10	-0.55	0.00

Specifically, the stacking periods of the Ba layers are 3 and 6 in the $P3_121$ - BaS_3 and T - BaS_3 structure, respectively {Supplemental Material Fig. S3(a) and (b) [43]}. Therefore, the S_3 units in BaS_3 have an effect on modulating the stacking sequence of Ba layers.

Motivated by the prediction and analysis of the new BaS_3 phase, we turned our attention to the BaS_2 compound. Li *et al.* [16] proposed a $P4_12_12$ - BaS_2 phase holding energetic and dynamical stability at a pressures range of 100 to 140 GPa. However, with the pressure increasing to 150 GPa, the $P4_12_12$ - BaS_2 phase becomes dynamically unstable. Commonly, the stability of one crystalline structure increases with pressure, thus it is intriguing to investigate the factor causing the dynamical instability of the BaS_2 structure at higher pressure. Fully geometrical optimizations were performed for the $P4_12_12$ - BaS_2 at 100 GPa and 150 GPa, respectively, to guarantee the structures lying in the local minimum of the PES at corresponding pressures. And at 150 GPa, BaS_2 undergoes a phase transition from $P4_12_12$ to $Fd-3m$ with a higher symmetry, which is also identical to our structural prediction results performed at 150 GPa (Supplemental Material Fig. S4 [43]). At 100 GPa, S atoms form the S_2 unit with an S-S bond length of about 2.01 Å, while at 150 GPa, the distance of ~ 2.30 Å between the two nearest S atoms [Fig. 2(d)] is much larger than 2.07 Å at ambient pressure. Generally, a higher pressure will decrease the atomic distance accompanying the enhancing interaction, while the S-S distance becomes larger in the BaS_2 compound. We calculated the phonon dispersion relations corresponding to the pressure of 150 GPa and projected them on both Ba and S atoms (Supplemental Material Fig. S5 [43]). It can be seen that the imaginary frequencies

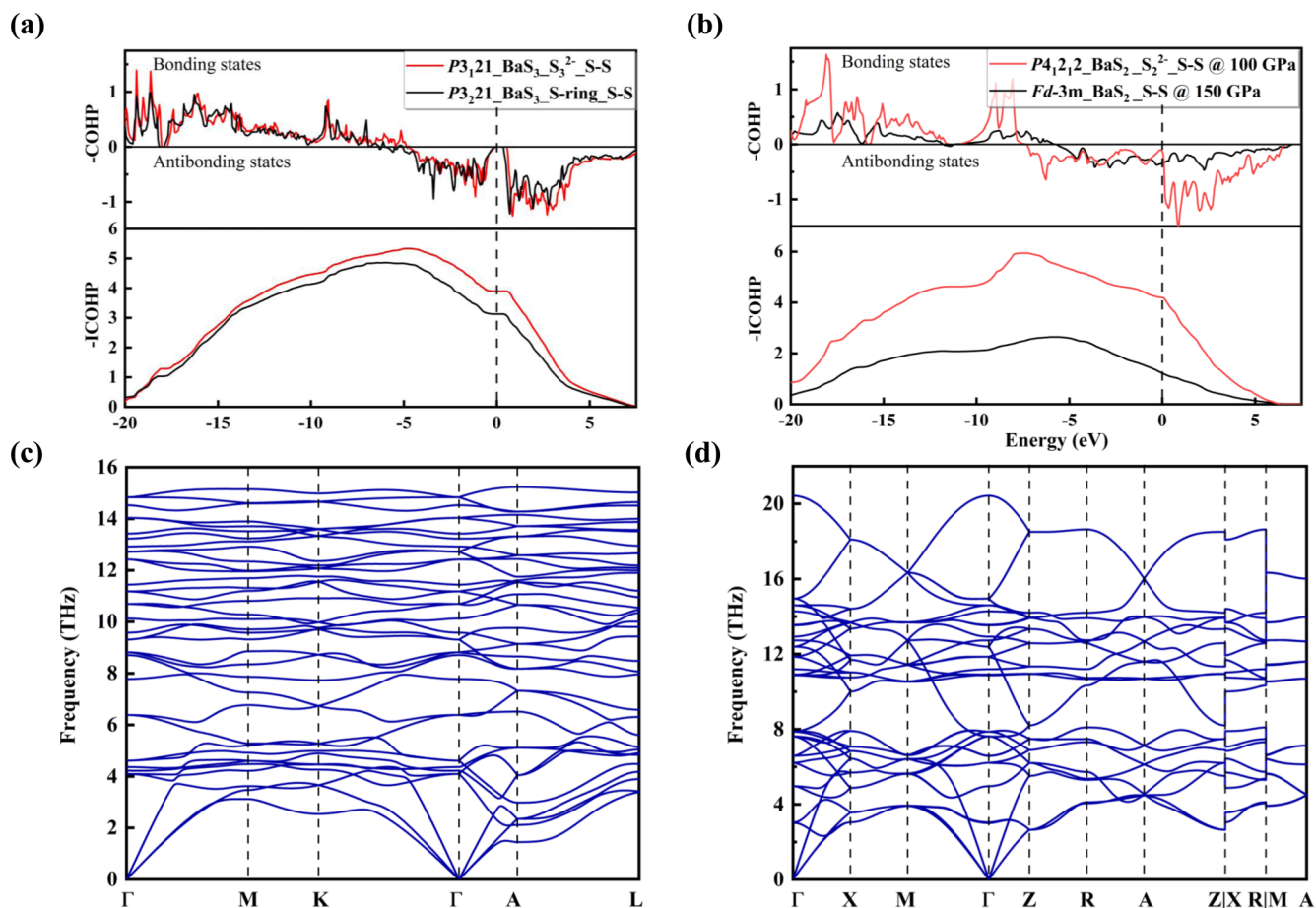


FIG. 3. The COHP and ICOHP analysis for the S-S bonding states of the (a) BaS₃ compound with $P3_121$ and $P3_21$ symmetry, and of the (b) $P4_12_12$ -BaS₂ compound at 100 GPa and $Fd-3m$ -BaS₂ at 150 GPa, respectively. The phonon dispersion relations of the (c) $P3_21$ -BaS₃ at a pressure of 100 GPa and temperature of 300 K, and (d) $Fd-3m$ -BaS₂ at a pressure of 150 GPa and temperature of 1000 K.

of the phonon spectrum are mainly attributed to the S atoms. Thus, we first calculated the COHP and ICOHP to reveal the difference between the S-S bonding states of the BaS₂ compound at 100 GPa and 150 GPa, respectively. As shown in Fig. 3(b), it is clearly seen that the negative ICOHP value of the bond at 150 GPa is much smaller than that at 100 GPa, indicating the interaction of the S—S bond becomes weaker at 150 GPa. We also calculated the ELF and depict it in Fig. 2(e), indicating there is no electron localizing along the S—S bond direction at a pressure of 150 GPa. Moreover, we performed the AIMD simulations for the $P4_12_12$ -BaS₂ structure at 150 GPa and at temperatures of 300, 500, and 1000 K, and the phonon dispersion relations of the BaS₂ compound at these three temperatures [Supplemental Material Fig. S6 [43] and Fig. 3(d)] were carried out from the AIMD simulation results using the TDEP method. As shown in Supplemental Material Fig. S6 [43], the phonon spectra of the structure at 300 K still have minor imaginary frequencies (red line) along the path from the gamma point to point X in the Brillouin zone. However, the phonon dispersions carried out from the simulation results at 1000 K have no imaginary frequency [Fig. 3(d)], confirming the higher temperature will contribute more to the dynamic stability of BaS₂. From this analysis, we may conclude that in the S-rich system, the S₃/S₂ units are con-

figurationally preferable than the atomic arrangement with a homogeneous distance, leaving a lower symmetry. Moreover, the existence of the S_x subunits may also be crucial for the stability of the Ba polysulfides, and we suggest that one may coarsely check the dynamical stability of the future findings of the BaS₂ compound using ELF or COHP simulation to replace the source demand phonon spectra calculation.

After the structural prediction of the BaS₃ and BaS₂ compounds, we further investigated the electronic properties of the $P3_121$ -BaS₃ phase. The energy band structure and projected density of states (PDOS) are shown in Fig. 4(a). The BaS₃ compound is an indirect band-gap semiconductor with an energy band gap of about 0.5 eV, which is about 0.3 eV lower than the calculated results using the Heyd-Scuseria-Ernzerhof hybrid functional (Supplemental Material Fig. S7 [43]), and the S-3*p*-orbital contributes most to the density of states (DOS) near the Fermi level. Moreover, we investigated the PDOS structure of the 3*p*-orbital of the S atoms in detail by separating the distribution of the electrons belonging to S1 and S2 atoms [Fig. 4(b)]. Near the Fermi energy level, the 3*p* electronic energy levels of the S1 atoms are higher than that of S2 atoms, indicating that the charge transfer from the Ba atoms mainly participates in the characterization of the bonding state between the S atoms. As is well known,

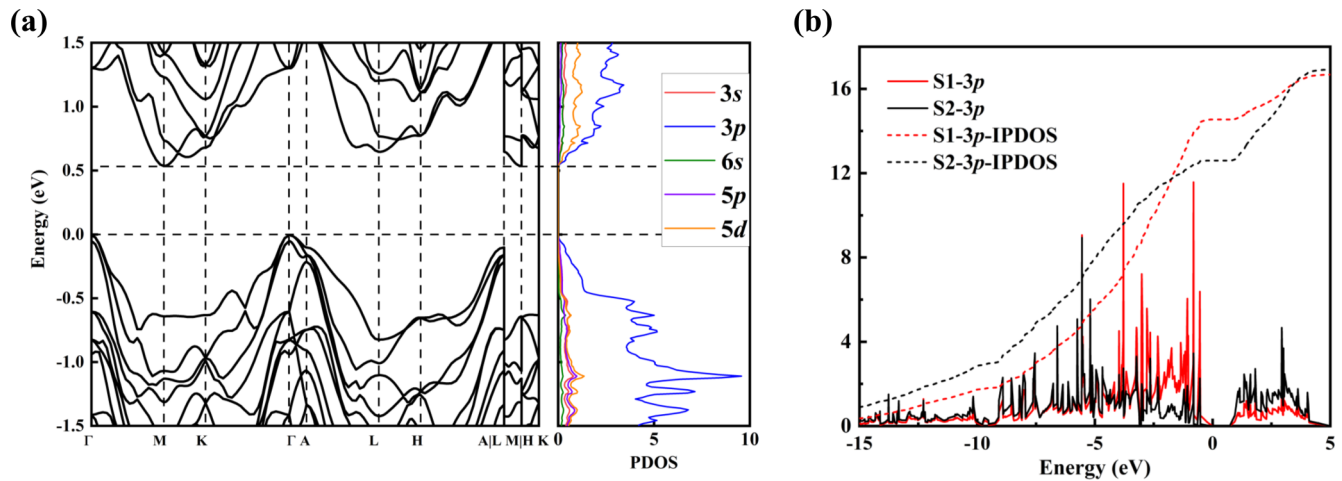


FIG. 4. (a) The simulated band structure and PDOS of $P3_21$ - BaS_3 and (b) the projected DOS to the $3p$ -orbital belonging to the S1 and S2 atoms of the BaS_3 compound at 100 GPa. IPDOS represents integrated PDOS.

the motif of the S configuration will influence the properties of the S-contained compound. Here we throw light on the evolution relation between the S-S-S angle and the band gap. As the pressure ranges from 50 and 70 GPa (Supplemental Material Fig. S8 [43]), the band gap of the $P42_1m$ - BaS_3 structure decreases slightly from 1.37 to 1.14 eV, with the S-S-S angle decreasing from 100.0° to 95.7° . At more than 70 GPa, BaS_3 undergoes a phase transition from $P42_1m$ to the $P3_21$ - BaS_3 structure, and the S-S-S angle decreases from 101.0° to 98.6° , accompanied by the band gap decreasing from 0.80 to 0.53 eV. To be noted, the S—S bond length almost remains unchanged with pressure. Therefore, we could conclude that the band gap will decrease with the S-S-S angle in the same crystalline structure.

IV. CONCLUSION

In summary, we performed structure searching for the BaS_3 and BaS_2 compounds up to 150 GPa using the CALYPSO method based on the ab initio calculations. We proposed a new BaS_3 phase with $P3_21$ symmetry at a pressure of 100 GPa by moving the S2 atoms along the eigenvector of the soft mode of the predicted $P3_21$ - BaS_3 phase. When

considering the instability of $P3_21$ - BaS_3 induced by the motivation of the S2 atoms, we further performed AIMD simulations at a finite temperature to estimate the temperature effect on the stability of the $P3_21$ - BaS_3 phase using the TDEP method. As expected, the higher temperature makes a contribution to its stability. We also investigated the stability of the BaS_2 compound crystallizing in $Fd\bar{3}m$ symmetry at a pressure of 150 GPa, pointing out that the absence of the S—S bond in BaS_2 induces the instability of the BaS_2 compound at a higher pressure. The finite temperature effect on the unstable BaS_2 compound at 150 GPa was also explored using the TDEP method, confirming the high-temperature contribution to phonon hardening. These findings have elaborated on the abundant Ba polysulfides, which may provide a prominent exemplification for future investigations of Ba-S systems.

ACKNOWLEDGMENTS

This research was supported by the National Natural Science Foundation of China under Grants No. 12174142, No. 12034009, and No. 12104176; the Program for JLU Science and Technology Innovative Research Team. Part of the calculation was performed in the high-performance computing center of Jilin University.

-
- [1] L. Zhu, H. Liu, C. J. Pickard, G. Zou, and Y. Ma, Reactions of xenon with iron and nickel are predicted in the earth's inner core, *Nat. Chem.* **6**, 644 (2014).
- [2] A. B. Altman, A. D. Tamerius, N. Z. Koocher, Y. Meng, C. J. Pickard, J. P. S. Walsh, J. M. Rondinelli, S. D. Jacobsen, and D. E. Freedman, Computationally directed discovery of MoBi_2 , *J. Am. Chem. Soc.* **143**, 214 (2021).
- [3] S. Shao, W. Zhu, J. Lv, Y. Wang, Y. Chen, and Y. Ma, The exotically stoichiometric compounds in Al-S system under high pressure, *npj Comput. Mater.* **6**, 11 (2020).
- [4] L. Zhang, Y. Wang, J. Lv, and Y. Ma, Materials discovery at high pressures, *Nat. Rev. Mater.* **2**, 17005 (2017).
- [5] Y. Li, J. Hao, H. Liu, Y. Li, and Y. Ma, The metallization and superconductivity of dense hydrogen sulfide, *J. Chem. Phys.* **140**, 174712 (2014).
- [6] D. Duan, Y. Liu, F. Tian, D. Li, X. Huang, Z. Zhao, H. Yu, B. Liu, W. Tian, and T. Cui, Pressure-induced metallization of dense $(\text{H}_2\text{S})_2\text{H}_2$ with high- T_c superconductivity, *Sci. Rep.* **4**, 6968 (2014).
- [7] A. P. Drozdov, M. I. Erements, I. A. Troyan, V. Ksenofontov, and S. I. Shylin, Conventional superconductivity at 203 Kelvin at high pressures in the sulfur hydride system, *Nature (London)* **525**, 73 (2015).
- [8] H. Liu, I. I. Naumov, R. Hoffmann, N. W. Ashcroft, and R. J. Hemley, Potential high- T_c superconducting lanthanum

- and yttrium hydrides at high pressure, *Proc. Natl. Acad. Sci. USA* **114**, 6990 (2017).
- [9] M. Somayazulu, M. Ahart, A. K. Mishra, Z. M. Geballe, M. Baldini, Y. Meng, V. V. Struzhkin, and R. J. Hemley, Evidence for Superconductivity Above 260 K in Lanthanum Superhydride at Megabar Pressures, *Phys. Rev. Lett.* **122**, 027001 (2019).
- [10] M. S. Miao, Caesium in high oxidation states and as a *p*-block element, *Nat. Chem.* **5**, 846 (2013).
- [11] G. Yang, Y. Wang, F. Peng, A. Bergara, and Y. Ma, Gold as a 6*p*-element in dense lithium aurides, *J. Am. Chem. Soc.* **138**, 4046 (2016).
- [12] J. Lin, X. Du, M. Rahm, H. Yu, H. Xu, and G. Yang, Exploring the limits of transition-metal fluorination at high pressures, *Angew. Chem. Int. Ed.* **59**, 9155 (2020).
- [13] J. Lin, Z. Zhao, C. Liu, J. Zhang, X. Du, G. Yang, and Y. Ma, IrF₈ molecular crystal under high pressure, *J. Am. Chem. Soc.* **141**, 5409 (2019).
- [14] C. Cao, R. E. Vernon, W. H. E. Schwarz, and J. Li, Understanding periodic and non-periodic chemistry in periodic tables, *Front. Chem.* **8**, 813 (2021).
- [15] D. Luo, Y. Wang, G. Yang, and Y. Ma, Barium in high oxidation states in pressure-stabilized barium fluorides, *J. Phys. Chem. C* **122**, 12448 (2018).
- [16] F. Li, X. Zhang, Y. Fu, Y. Wang, A. Bergara, and G. Yang, Ba with unusual oxidation states in Ba chalcogenides under pressure, *J. Phys. Chem. Lett.* **12**, 4203 (2021).
- [17] M. J. Greschner, D. D. Klug, and Y. Yao, Prediction of a stable half-metal ferromagnetic BaCl solid, *Phys. Rev. B* **93**, 094428 (2016).
- [18] W. Meng, B. Saparov, F. Hong, J. Wang, D. B. Mitzi, and Y. Yan, Alloying and defect control within chalcogenide perovskites for optimized photovoltaic application, *Chem. Mater.* **28**, 821 (2016).
- [19] R. J. Zollweg, Optical absorption and photoemission of barium and strontium oxides, sulfides, selenides, and tellurides, *Phys. Rev.* **111**, 113 (1958).
- [20] N. Gross, Y. Y. Sun, S. Perera, H. Hui, X. Wei, S. Zhang, H. Zeng, and B. A. Weinstein, Stability and Band-Gap Tuning of the Chalcogenide Perovskite BaZrS₃ in Raman and Optical Investigations at High Pressures, *Phys. Rev. Appl.* **8**, 044014 (2017).
- [21] Y. Wang, M. Xu, L. Yang, B. Yan, Q. Qin, X. Shao, Y. Zhang, D. Huang, X. Lin, J. Lv, D. Zhang, H. Gou, H. Kwang Mao, C. Chen, and Y. Ma, Pressure-stabilized divalent ozonide CaO₃ and its impact on Earth's oxygen cycles, *Nat. Commun.* **11**, 4702 (2020).
- [22] Y. Liu, C. Wang, S. Han, X. Chen, H. Sun, and X. Liu, Novel superconducting electrides in Ca–S system under high pressures, *Chin. Phys. Lett.* **38**, 036201 (2021).
- [23] S. Wang, W. Lu, S. Liu, M. Zhou, P. Gao, H. Wang, J. Lv, H. Gou, G. Liu, H. Liu, Y. Wang, and Y. Ma, Synthesis of calcium polysulfides at high pressures, *Phys. Rev. B* **104**, 054117 (2021).
- [24] M. Llunell, P. Alemany, and I. D. P. R. Moreira, Electronic structure and magnetic properties of potassium ozonide KO₃, *Inorg. Chem.* **48**, 5938 (2009).
- [25] C. W. Mandeville, Sulfur: A ubiquitous and useful tracer in earth and planetary sciences, *Elements* **6**, 75 (2010).
- [26] G. Liu, Z. Yu, H. Liu, S. A. T. Redfern, X. Feng, X. Li, Y. Yuan, K. Yang, N. Hirao, S. I. Kawaguchi, X. Li, L. Wang, and Y. Ma, Unexpected semimetallic BiS₂ at high pressure and high temperature, *J. Phys. Chem. Lett.* **9**, 5785 (2018).
- [27] P. Rejmak, Structural, optical, and magnetic properties of ultramarine pigments: A DFT insight, *J. Phys. Chem. C* **122**, 29338 (2018).
- [28] G. S. Pokrovski and L. S. Dubrovinsky, The S₃[−] ion is stable in geological fluids at elevated temperatures and pressures, *Science* **311**, 1052 (2011).
- [29] B. Meyer, Elemental sulfur, *Chem. Rev.* **76**, 367 (1976).
- [30] Y. Wang, J. Lv, L. Zhu, and Y. Ma, Crystal structure prediction via particle-swarm optimization, *Phys. Rev. B* **82**, 094116 (2010).
- [31] Y. Wang, J. Lv, L. Zhu, and Y. Ma, CALYPSO: a method for crystal structure prediction, *Comput. Phys. Commun.* **183**, 2063 (2012).
- [32] F. Peng, Y. Sun, C. J. Pickard, R. J. Needs, Q. Wu, and Y. Ma, Hydrogen Clathrate Structures in Rare Earth Hydrides at High Pressures: Possible Route to Room-Temperature Superconductivity, *Phys. Rev. Lett.* **119**, 107001 (2017).
- [33] H. Wang, J. S. Tse, K. Tanaka, T. Iitaka, and Y. Ma, Superconductive sodalite-like clathrate calcium hydride at high pressures, *Proc. Natl. Acad. Sci. USA* **109**, 6463 (2012).
- [34] X. Zhang, Y. Zhao, and G. Yang, Superconducting ternary hydrides under high pressure, *Wiley Interdiscip. Rev. Comput. Mol. Sci.* (2021).
- [35] P. E. Blöchl, Projector augmented-wave method, *Phys. Rev. B* **50**, 17953 (1994).
- [36] J. P. Perdew, K. Burke, and M. Ernzerhof, Generalized Gradient Approximation Made Simple, *Phys. Rev. Lett.* **77**, 3865 (1996).
- [37] G. Kresse and J. Furthmüller, Efficient iterative schemes for ab initio total-energy calculations using a plane-wave basis set, *Phys. Rev. B* **54**, 11169 (1996).
- [38] K. Parlinski, Z. Q. Li, and Y. Kawazoe, First-Principles Determination of the Soft Mode in Cubic ZrO₂, *Phys. Rev. Lett.* **78**, 4063 (1997).
- [39] A. Togo, F. Oba, and I. Tanaka, First-principles calculations of the ferroelastic transition between rutile-type and CaCl₂-type SiO₂ at high pressures, *Phys. Rev. B* **78**, 134106 (2008).
- [40] O. Hellman, I. A. Abrikosov, and S. I. Simak, Lattice dynamics of anharmonic solids from first principles, *Phys. Rev. B* **84**, 180301(R) (2011).
- [41] O. Hellman and I. A. Abrikosov, Temperature-dependent effective third-order interatomic force constants from first principles, *Phys. Rev. B* **88**, 144301 (2013).
- [42] O. Hellman, P. Steneteg, I. A. Abrikosov, and S. I. Simak, Temperature dependent effective potential method for accurate free energy calculations of solids, *Phys. Rev. B* **87**, 104111 (2013).
- [43] See Supplemental Material at <http://link.aps.org/supplemental/10.1103/PhysRevResearch.4.023046> for computational details, results of the structure prediction of the 6 f.u. unit cell, supporting figures and structure information.